

## Supporting Information

### **Self-supported bifunctional MoNi<sub>4</sub> framework by iron doping for ultra-efficient water splitting**

Xiangyuan Zhao, Kewei Tang, Xiaomei Wang, Weihong Qi, Hong Yu, Cheng-Feng Du\*, Qian Ye\*

State Key Laboratory of Solidification Processing, Center of Advanced Lubrication and Seal Materials, School of Materials Science and Engineering, Northwestern Polytechnical University, Xi'an, ShaanXi, 710072, China

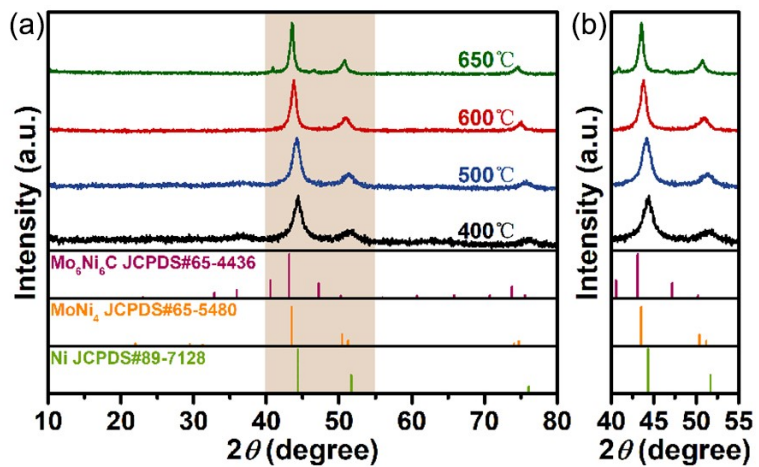


Fig. S1 The XRD pattern of the  $\text{MNF}_{2.5}$  CFs samples treated under different temperature from 400 °C to 650 °C. (a) XRD patterns, (b) magnified XRD patterns in the  $2\theta$  range from 40° to 55°.

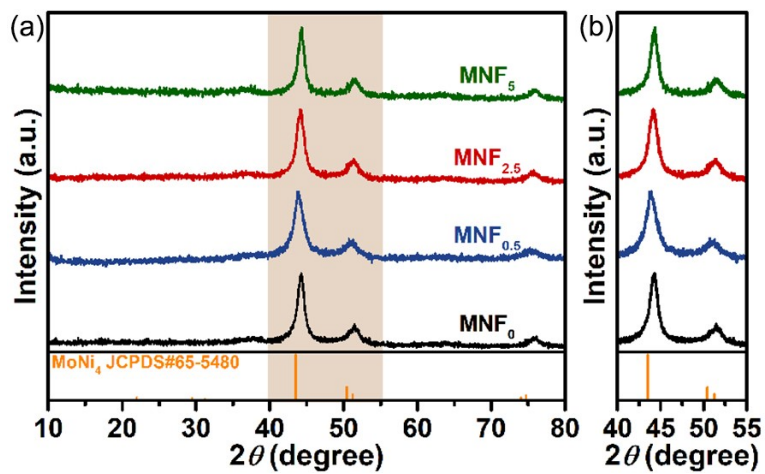


Fig. S2 The XRD patterns of  $\text{MNF}_n$  CFs samples with various Fe addition treated under 500 °C. (a) XRD patterns, (b) magnified XRD patterns in the  $2\theta$  range from 40° to 55°.

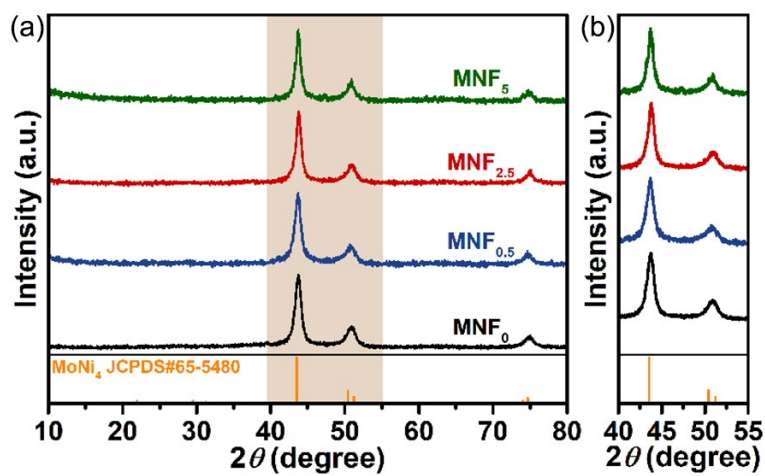


Fig. S3 The XRD patterns of  $\text{MNF}_n$  CFs samples with different Fe addition, which were treated at 600 °C. (a) XRD patterns, (b) magnified XRD patterns in the  $2\theta$  range from 40° to 55°.

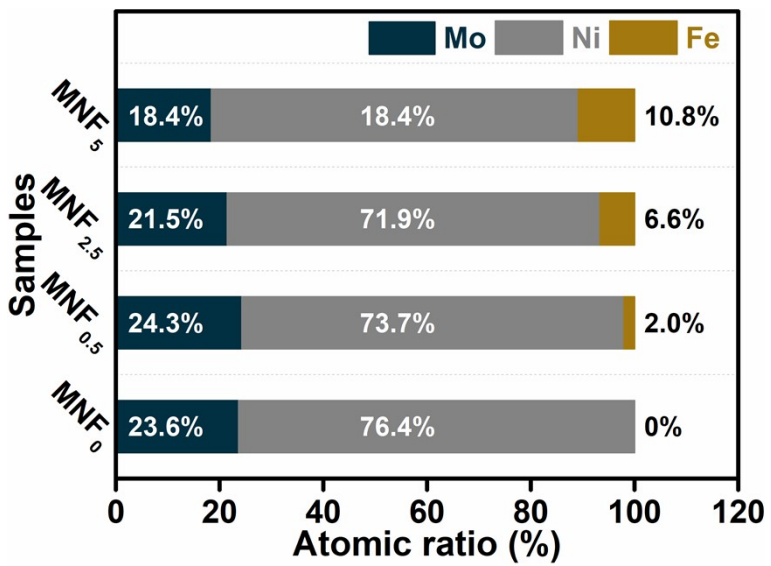


Fig. S4 The elemental ratios of Mo, Ni, and Fe in the series of  $\text{MNF}_n$  CFs samples by ICP-OES.

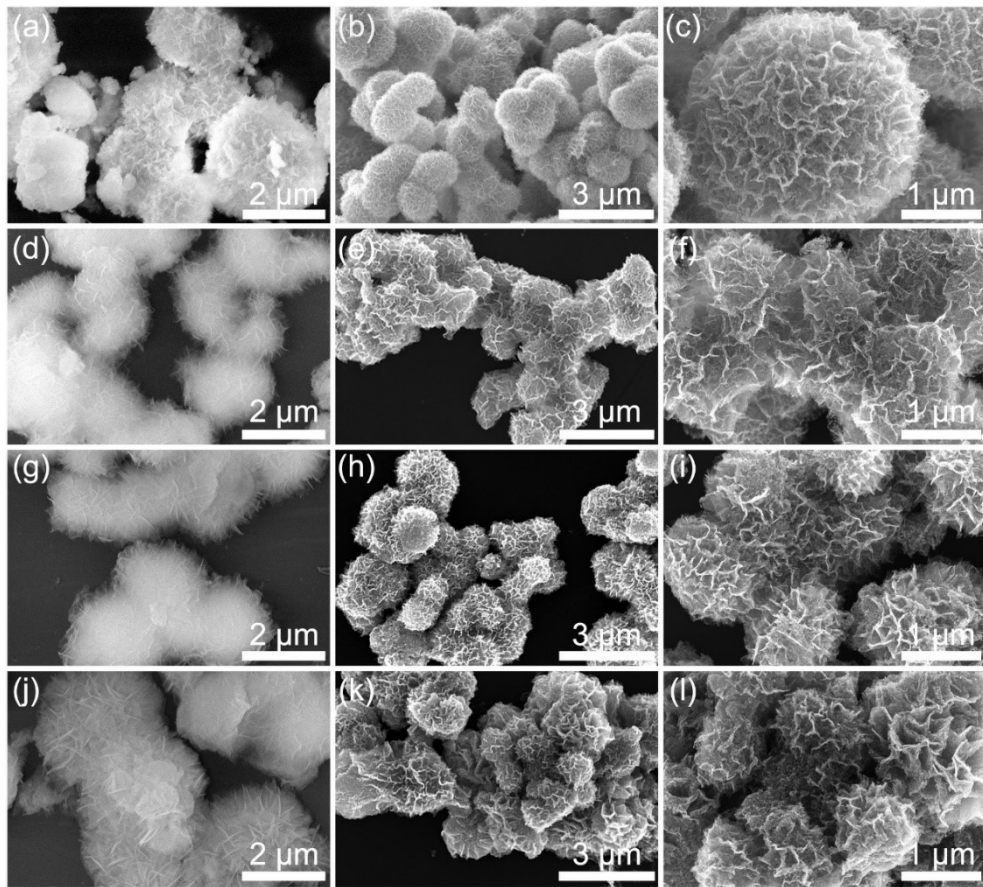


Fig. S5 The SEM images of  $\text{MNF}_n$  CFs samples with different Fe addition, which were treated at 500 °C. (a)  $\text{MNF}_0$  precursor and (b-c)  $\text{MNF}_0$ , (d)  $\text{MNF}_{0.5}$  precursor and (e-f)  $\text{MNF}_{0.5}$ , (g)  $\text{MNF}_{2.5}$  precursor and (h-i)  $\text{MNF}_{2.5}$ , and (j)  $\text{MNF}_5$  precursor and (k-l)  $\text{MNF}_5$  CFs.

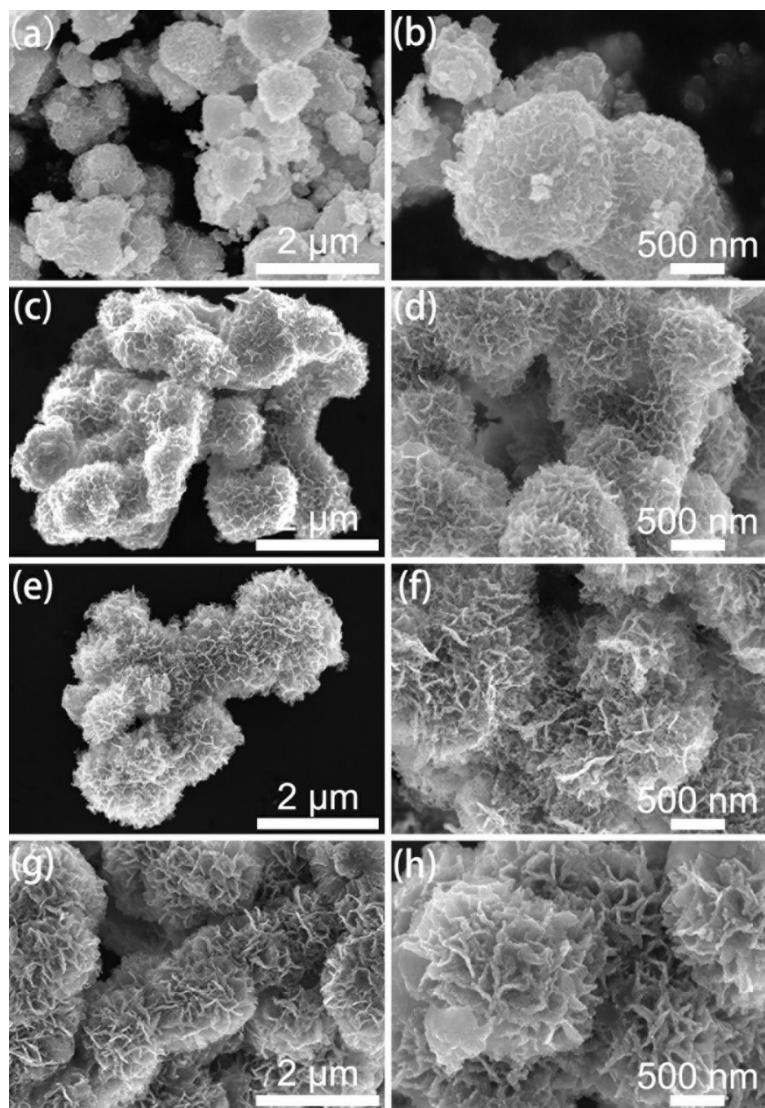


Fig. S6 The SEM images of  $\text{MNF}_n$  CFs samples with different Fe addition, which were treated at 600 °C. (a-b)  $\text{MNF}_0$ , (c-d)  $\text{MNF}_{0.5}$ , (e-f)  $\text{MNF}_{2.5}$ , and (g-h)  $\text{MNF}_5$  CFs.

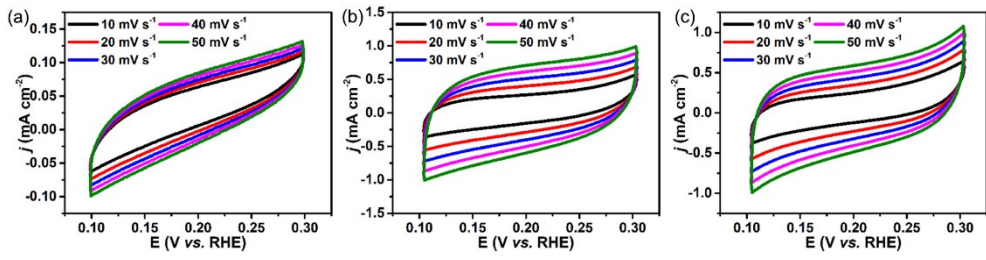


Fig. S7 Cyclic voltammograms (CV) curves of the  $\text{MNF}_{2.5}$  CFs samples treated at (a) 400 °C, 500 °C, and (b) 600°C, which were measured at various scan rates of 10, 20, 30, 40, and 50  $\text{mV s}^{-1}$  in 1 M KOH solution.

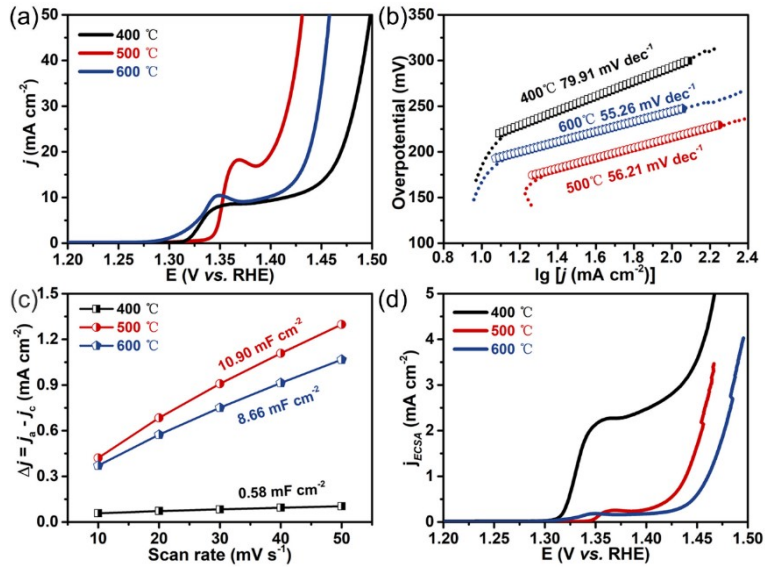


Fig. S8 (a) LSV curves of MNF<sub>2.5</sub> CFs samples treated at the temperature range from 400 °C to 600 °C in 1M KOH at a scan rate of 1 mV s<sup>-1</sup>, (b) corresponding Tafel plots of the series of MNF<sub>2.5</sub> CFs samples, (c)  $C_{dl}$  values of the different MNF<sub>2.5</sub> CFs samples, (d) normalized LSV curves by ECSA.

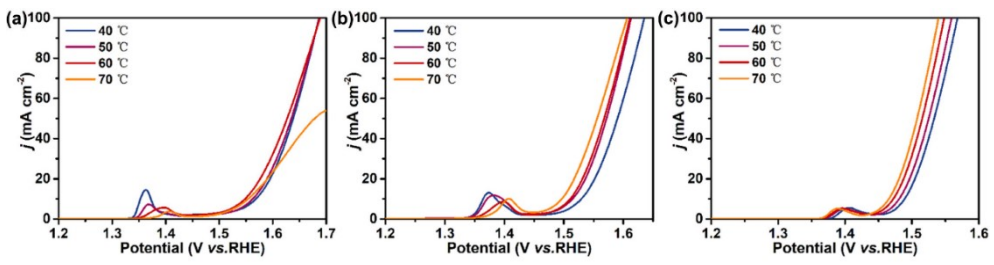


Fig. S9 OER polarization curves of the (a) MNF<sub>0</sub>, (b) MNF<sub>0.5</sub>, and (c) MNF<sub>5</sub> CFs samples in the 1 M KOH aqueous electrolyte at different temperatures from 40 °C to 70 °C.

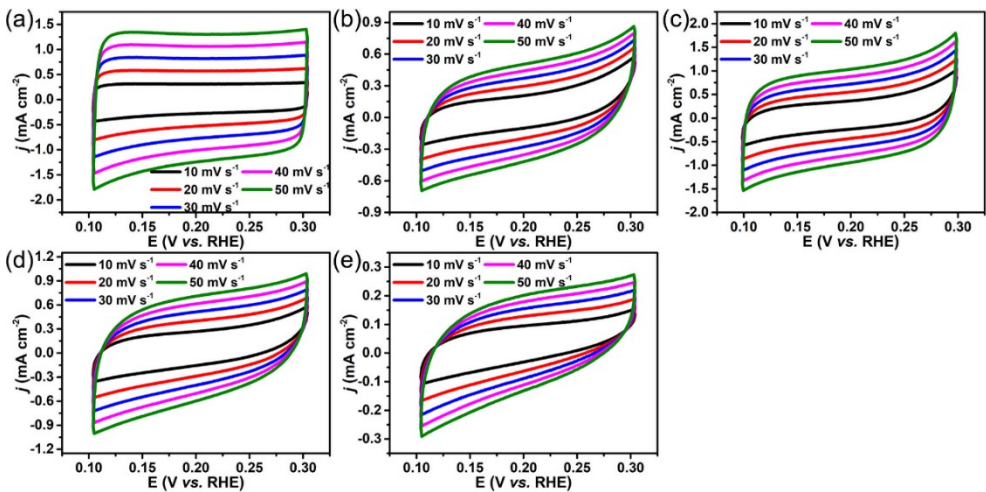


Fig. S10 Cyclic voltammograms (CV) curves of (a)  $\text{IrO}_2$  catalyst, (b-e) the  $\text{MNF}_0$ ,  $\text{MNF}_{0.5}$ ,  $\text{MNF}_{2.5}$ , and  $\text{MNF}_5$  CFs samples treated at  $500\text{ }^\circ\text{C}$ , which were measured at various scan rates of 10, 20, 30, 40, and  $50\text{ mV s}^{-1}$  in 1 M KOH solution.

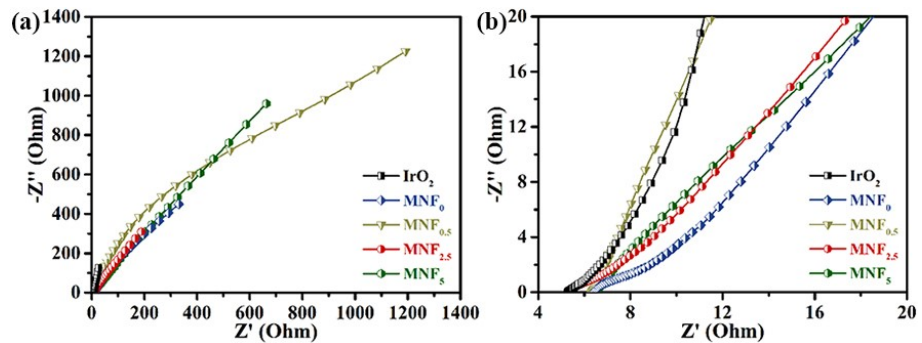


Fig. S11 The EIS spectra (a) and enlarged spectra (b) of  $\text{IrO}_2$  and  $\text{MNF}_{2.5}$  CFs in 1M KOH.

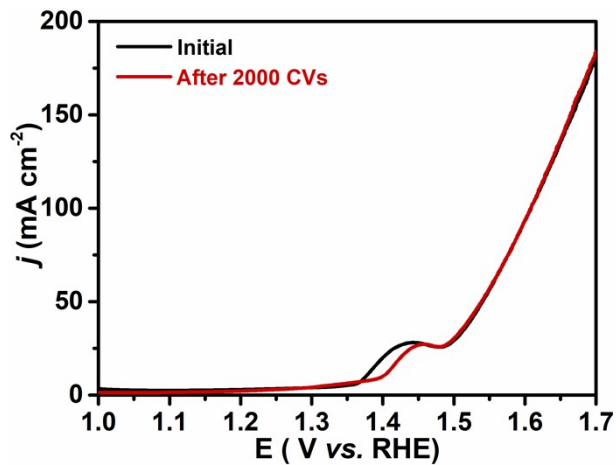


Fig. S12 Polarization curves of  $\text{MNF}_{2.5}$  CFs sample before and after 2000 CV cycles.

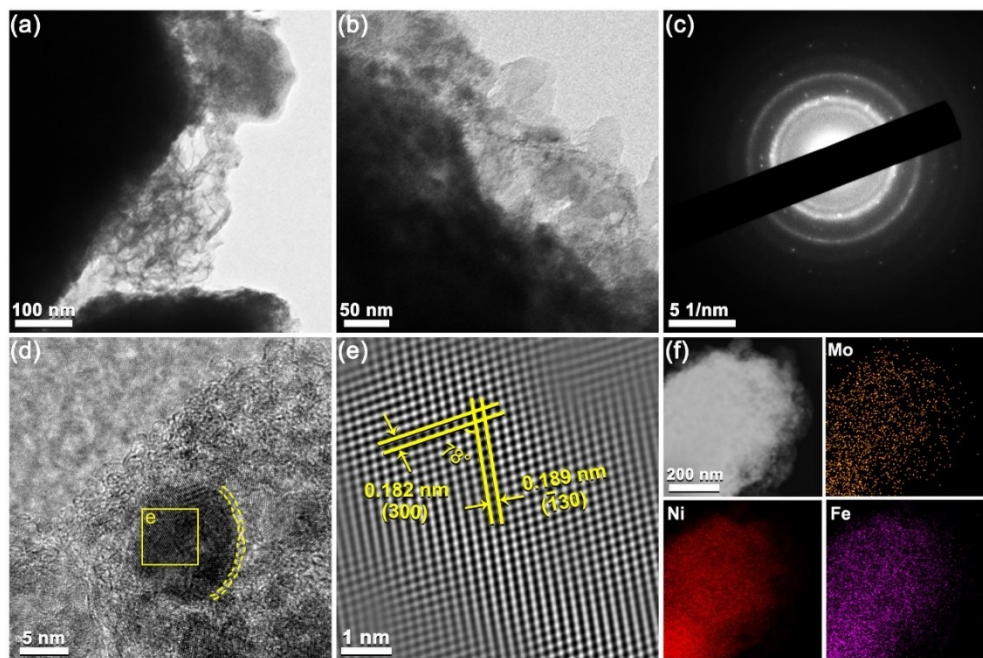


Fig. S13 The TEM images of  $\text{MNF}_{2.5}$  CFs catalyst treated at 500°C after OER stability test process. (a) and (b) TEM, (c) SAED pattern, (d) HRTEM, (e) the inverse-FFT image of highlighted block in (d), and (f) the EDX elemental mapping.

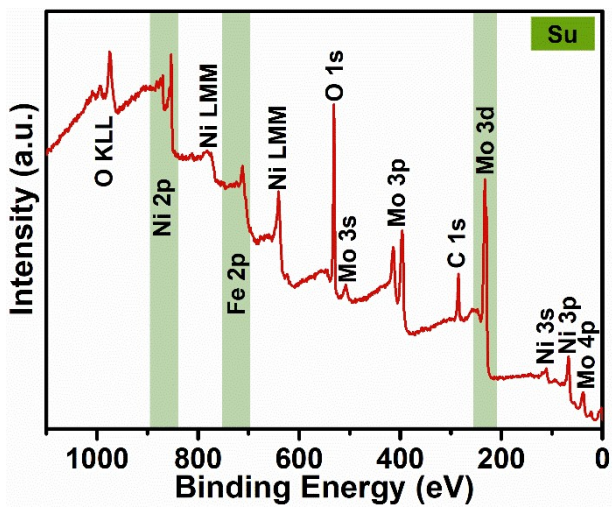


Fig. S14 The Survey XPS spectrum of the  $\text{MNF}_{2.5}$  CFs sample treated at 500 °C.

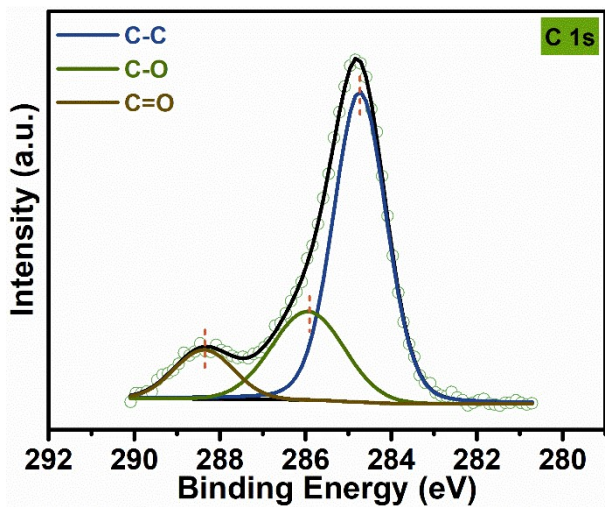


Fig. S15 High-resolution XPS spectrum of C 1s of  $\text{MNF}_{2.5}$  CFs sample treated at 500  $^{\circ}\text{C}$ .

The peaks at 284.75, 285.45, and 288.46 eV can be recognized to C-C, C-O, and C=O bonds, respectively.<sup>1</sup>

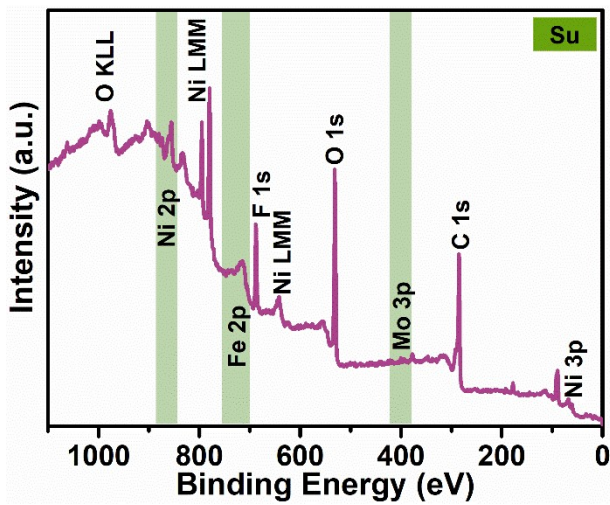


Fig. S16 The Survey XPS spectrum of the  $\text{MNF}_{2.5}$  CFs sample after OER measurement.

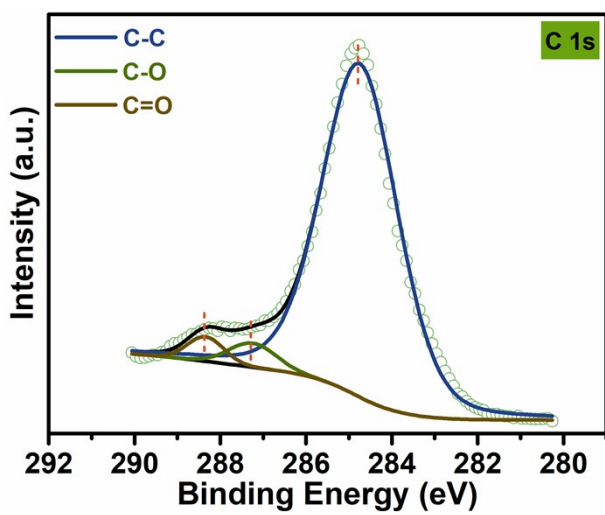


Fig. S17 High-resolution XPS spectrum of C 1s of  $\text{MNF}_{2.5}$  CFs sample after OER measurement.

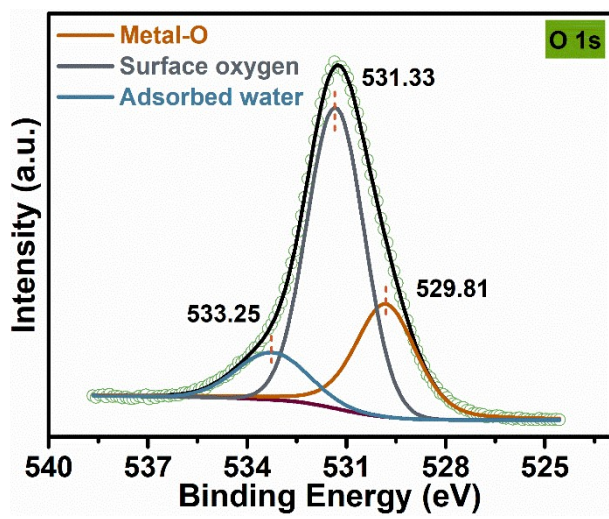


Fig. S18 High-resolution XPS spectrum of O 1s of  $\text{MNF}_{2.5}$  CFs sample after OER measurement.

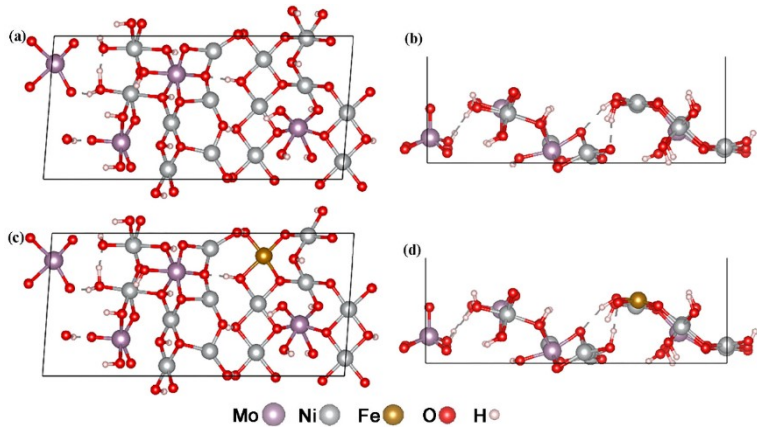
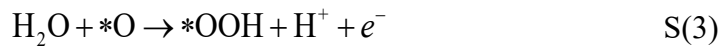


Fig. S19 Top (a) and side (b) view of MoNiOOH, top (c) and side (d) view of MoNiFeOOH.

Eq. S(1) - S(4) were adopted to express the mechanism of OER, as the four-electron transfer reaction pathway in the calculation.



Here, the \* represents the catalytic active sites on the surface of the samples, and the oxygen-containing groups (\*OH, \*O, and \*OOH) express the adsorbed intermediates on the active sites.

The free energy of the adsorbed intermediates was calculated based on the standard hydrogen electrode, defined as Eq. S(5), where  $E$ ,  $ZPE$ ,  $\Delta H_t$ ,  $T$ , and  $S$  represented the total energy, zero-point energy, the change in the heat capacity, thermal correction energy (298.15 K), and entropy, respectively. The Gibbs free energy in the OER process were obtained according to the formulas Eq. S(5) – S(12).

$$G = E + ZPE + \Delta H_t - T \cdot S \quad \text{S(5)}$$

$$ZPE = \frac{\hbar}{2} \sum_{i=1}^{3N} v_i \quad \text{S(6)}$$

$$\Delta H_t = \sum_{i=1}^{3N} \frac{hv_i}{e^{\frac{hv_i}{k_B T}} - 1} \quad S(7)$$

$$T \cdot S = \sum_{i=1}^{3N} \left[ \frac{hv_i}{e^{\frac{hv_i}{k_B T}} - 1} - k_B T \ln \left( 1 - e^{-\frac{hv_i}{k_B T}} \right) \right] \quad S(8)$$

$$\Delta G_1 = G(*OH) + \frac{1}{2}G(H_2) - G(H_2O) - G(*) - eU - k_B T \ln(10) \times pH \quad S(9)$$

$$\Delta G_2 = G(*O) + \frac{1}{2}G(H_2) - G(*OH) - eU - k_B T \ln(10) \times pH \quad S(10)$$

$$\Delta G_3 = G(*OOH) + \frac{1}{2}G(H_2) - G(H_2O) - G(*O) - eU - k_B T \ln(10) \times pH \quad S(11)$$

$$\Delta G_4 = 4.92 \text{ eV} - \sum_{i=1}^3 \Delta G_i(0,0) - eU - k_B T \ln(10) \times pH \quad S(12)$$

Where  $U$ ,  $e$ , and  $k_B$  is the applied electrode potential, the charge transferred, the Boltzmann constant, respectively.

The overpotential ( $\eta$ ) was defined as below:

$$\eta = \max \{ \Delta G_1, \Delta G_2, \Delta G_3, \Delta G_4 \} / e - 1.23 \text{ V} \quad S(13)$$

Here, 1.23 V represents the balanced potential.<sup>2</sup>

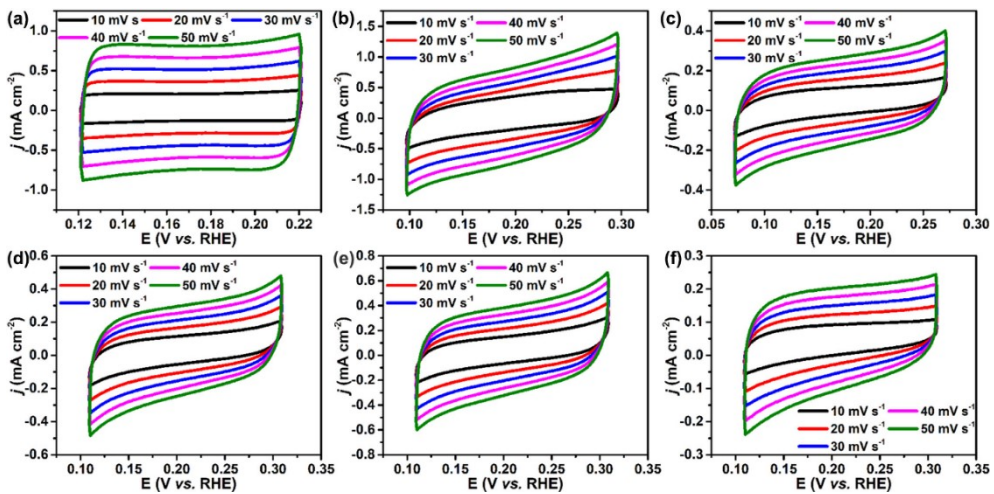


Fig. S20 Cyclic voltammograms (CV) curves of (a) 10 wt.% Pt/C catalyst, (b) MNF<sub>2.5</sub> CFs annealed at 500 °C, (c-f) MNF<sub>0</sub>, MNF<sub>0.5</sub>, MNF<sub>2.5</sub>, and MNF<sub>5</sub> CFs treated at 600 °C, which were measured at various scan rates of 10, 20, 30, 40, and 50 mV s<sup>-1</sup> in 1 M KOH solution before HER.

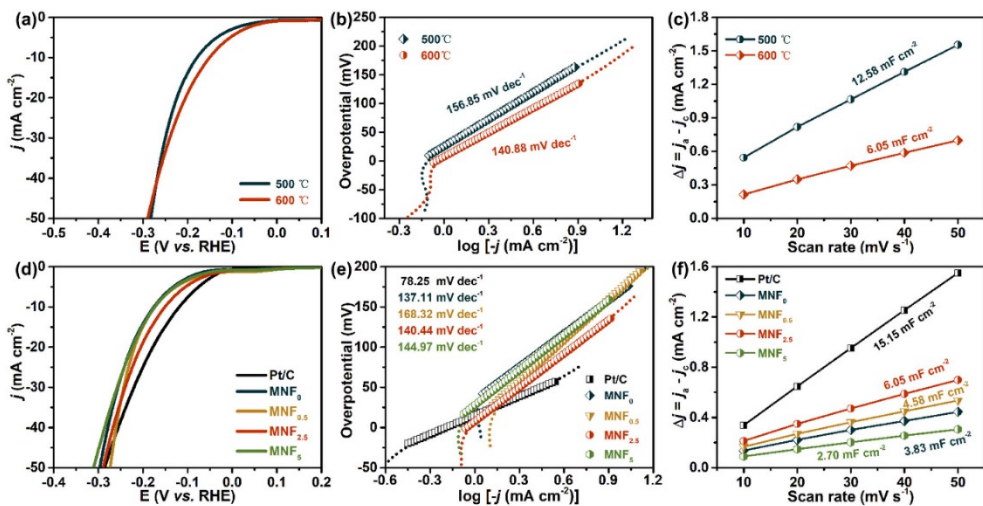


Fig. S21 (a) LSV curves, (b) Tafel plots, and (c)  $C_{\text{dl}}$  values of  $\text{MNF}_{2.5}\text{-}500$  CFs and  $\text{MNF}_{2.5}\text{-}600$  CFs. (d) LSV curves, (e) Tafel plots, and (f)  $C_{\text{dl}}$  values of the  $\text{MNF}_n$  CFs samples treated at the temperature of 600 °C.

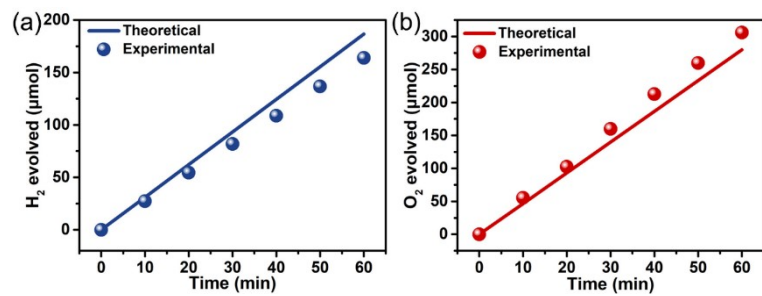


Fig. S22 The amounts of (a)  $\text{H}_2$  and (b)  $\text{O}_2$  theoretically calculated and experimentally measured versus time.

Table S1. Comparison of the OER performance of  $\text{MNF}_{2.5}$  CFs treated at 500 °C with other reported OER electrocatalysts in 1 M KOH electrolyte.

Electrocatalysts	Electrolyte	Overpotential (mV) at 30 mA cm <sup>-2</sup>	Tafel slope (mV dec <sup>-1</sup> )	References
$\text{MNF}_{2.5}$ -500 CFs	1M KOH	188	56.5	This work
N-WS <sub>2</sub> /Ni <sub>3</sub> FeN	1M KOH	220	55	<sup>3</sup>
TiO <sub>2</sub> @Co <sub>9</sub> S <sub>8</sub>	1M KOH	270	55	<sup>4</sup>
$\text{Ni}_{0.83}\text{Fe}_{0.17}(\text{OH})_2$	1M KOH	290	61	<sup>5</sup>
B,N:Mo <sub>2</sub> C@BCN	1M KOH	320	61	<sup>6</sup>
Co–Ni/Ni <sub>3</sub> N	1M KOH	350	63	<sup>7</sup>
NiMo-FG	1M KOH	370	67	<sup>8</sup>
Co@N-CS/N-HCP@CC	1M KOH	290	68	<sup>9</sup>
CoTeNR/NF	1M KOH	330	75	<sup>10</sup>
Ni–Co–P HNBs	1M KOH	310	76	<sup>11</sup>
FeCo-LDH/MXene	1M KOH	315	85	<sup>12</sup>
TTL	1M KOH	420	98.4	<sup>13</sup>
$\text{Ni}_{11}(\text{HPO}_3)_8(\text{OH})_6/\text{NF}$	1M KOH	290	102	<sup>14</sup>
$\text{NiCo}_2\text{O}_4@\text{CoMoO}_4/\text{NF}-7$	1M KOH	340	102	<sup>15</sup>
Co@HMNC	1M KOH	370	110	<sup>16</sup>
NiMoN/NF-450	1M KOH	310	116	<sup>17</sup>

Table S2. Comparison of the electrocatalytic activity of  $\text{MNF}_{2.5}$  CFs for overall water splitting with other recently reported bifunctional catalysts.

Electrode pair	Electrolyte	Overall voltage (V) at 20 mA cm <sup>-2</sup>	References
$\text{MNF}_{2.5}$ CFs	1M KOH	1.57	This work
$\text{RuCoO}_x$	1M KOH	1.58	<sup>18</sup>
$\text{Ni}_2\text{P}-\text{Ru}_2\text{P}/\text{NF}$	1M KOH	1.58	<sup>19</sup>
$\text{Ni}_2\text{P}@\text{NSG}$	1M KOH	1.60	<sup>20</sup>
$\text{Ti}_3\text{C}_2@\text{mNiCoP}$	1M KOH	1.61	<sup>21</sup>
Co-NiMoN-400	1M KOH	1.62	<sup>22</sup>
CoP-HS	1M KOH	1.63	<sup>23</sup>
Co–Ni/ $\text{Ni}_3\text{N}$	1M KOH	1.65	<sup>7</sup>
O-NiMoP/NF	1M KOH	1.68	<sup>24</sup>
$\text{Mo}_{0.6}\text{Ni}_{0.4}$	1M KOH	1.72	<sup>25</sup>
$\text{NiCo}_2\text{S}_4/\text{CC}$	1M KOH	1.73	<sup>26</sup>
Co/Ni-CW	1M KOH	1.79	<sup>27</sup>

## Reference

1. Y. Deng, X. Xi, Y. Xia, Y. Cao, S. Xue, S. Wan, A. Dong and D. Yang, *Adv. Mater.*, 2022, **34**, 2109145.
2. H. Xu, D. Cheng, D. Cao and X. C. Zeng, *Nat. Catal.*, 2018, **1**, 339-348.
3. J. Zeng, L. Zhang, Q. Zhou, L. Liao, Y. Qi, H. Zhou, D. Li, F. Cai, H. Wang, D. Tang and F. Yu, *Small*, 2022, **18**, 2104624.
4. S. Deng, Y. Zhong, Y. Zeng, Y. Wang, X. Wang, X. Lu, X. Xia and J. Tu, *Adv. Sci.*, 2018, **5**, 1700772.
5. Q. Zhou, Y. P. Chen, G. Q. Zhao, Y. Lin, Z. W. Yu, X. Xu, X. L. Wang, H. K. Liu, W. P. Sun and S. X. Dou, *ACS Catal.*, 2018, **8**, 5382-5390.
6. M. A. R. Anjum, M. H. Lee and J. S. Lee, *ACS Catal.*, 2018, **8**, 8296-8305.
7. K. Wang, Y. Guo, Z. Chen, D. Wu, S. Zhang, B. Yang and J. Zhang, *InfoMat*, 2021, **4**, 1-12.
8. S. Jeong, K. L. Hu, T. Ohto, Y. Nagata, H. Masuda, J. Fujita and Y. Ito, *ACS Catal.*, 2020, **10**, 792-799.
9. Z. L. Chen, Y. Ha, H. X. Jia, X. X. Yan, M. Chen, M. Liu and R. B. Wu, *Adv. Energy Mater.*, 2019, **9**, 1803918.
10. L. Yang, H. X. Xu, H. B. Liu, D. J. Cheng and D. P. Cao, *Small Methods*, 2019, **3**, 1900113.
11. E. L. Hu, Y. F. Feng, J. W. Nai, D. Zhao, Y. Hu and X. W. Lou, *Energy Environ. Sci.*, 2018, **11**, 872-880.
12. M. Tian, Y. Jiang, H. Tong, Y. Xu and L. Xia, *ChemNanoMat*, 2019, **6**, 154-159.
13. N. Hao, Y. Wei, J. Wang, Z. Wang, Z. Zhu, S. Zhao, M. Han and X. Huang, *RSC Adv.*, 2018, **8**, 20576-20584.
14. P. W. Menezes, C. Panda, S. Loos, F. Bunschei-Brunns, C. Walter, M. Schwarze, X. H. Deng, H. Dau and M. Driess, *Energy Environ. Sci.*, 2018, **11**, 1287-1298.
15. Y. Q. Gong, Z. Yang, Y. Lin, J. L. Wang, H. L. Pan and Z. F. Xu, *J. Mater. Chem. A*, 2018, **6**, 16950-16958.
16. H. Wang, Y. Jiao, S. Wang, P. Ye, J. Ning, Y. Zhong and Y. Hu, *Small*, 2021, **17**, 2103517.
17. Y. Wang, Y. Sun, F. Yan, C. L. Zhu, P. Gao, X. T. Zhang and Y. J. Chen, *J. Mater. Chem. A*, 2018, **6**, 8479-8487.
18. C. Zhou, S. Zhao, H. Meng, Y. Han, Q. Jiang, B. Wang, X. Shi, W. Zhang, L. Zhang and R. Zhang, *Nano Lett.*, 2021, **21**, 9633-9641.
19. S. Yang, J.-Y. Zhu, X.-N. Chen, M.-J. Huang, S.-H. Cai, J.-Y. Han and J.-S. Li, *Appl. Catal., B: Environ.*, 2022, **304**, 120914.
20. U. P. Suryawanshi, U. V. Ghorpade, D. M. Lee, M. R. He, S. W. Shin, P. V. Kumar, J. S. Jang, H. R. Jung, M. P. Suryawanshi and J. H. Kim, *Chem. Mater.*, 2021, **33**, 234-245.
21. Q. Yue, J. Sun, S. Chen, Y. Zhou, H. Li, Y. Chen, R. Zhang, G. Wei and Y. Kang, *ACS Appl. Mater. Interfaces*, 2020, **12**, 18570-18577.
22. Z. Yin, Y. Sun, Y. Jiang, F. Yan, C. Zhu and Y. Chen, *ACS Appl. Mater. Interfaces*, 2019, **11**, 27751-27759.
23. W. Zhang, N. Han, J. Luo, X. Han, S. Feng, W. Guo, S. Xie, Z. Zhou, P. Subramanian, K. Wan, J. Arbiol, C. Zhang, S. Liu, M. Xu, X. Zhang and J. Fransaer, *Small*, 2022, **18**, 2103561.
24. H. Jiang, M. Z. Sun, S. L. Wu, B. L. Huang, C. S. Lee and W. J. Zhang, *Adv. Funct. Mater.*, 2021, **31**, 2104951.
25. T. T. Zhang, X. W. Liu, X. Cui, M. L. Chen, S. J. Liu and B. Y. Geng, *Adv. Mater. Interfaces*, 2018, **5**, 1800359.

26. W. Song, M. Xu, X. Teng, Y. Niu, S. Gong, X. Liu, X. He and Z. Chen, *Nanoscale*, 2021, **13**, 1680-1688.
27. W. T. Gan, L. P. Wu, Y. X. Wang, H. Gao, L. K. Gao, S. L. Xiao, J. Q. Liu, Y. J. Xie, T. Li and J. Li, *Adv. Funct. Mater.*, 2021, **31**, 2010951.